CONF-8905118--7

2nd International Conference on
"Trends in Welding Research"
May 14-18, 1989, Gatlinburg, TN

Nd: YAG LASER WELDABILITY OF RS/PM AL-8FE-2MO SHEET

SAND--89-1317C

DE89 013588

S. Krishnaswamy and W. A. Baeslack III
Department of Welding Engineering
The Ohio State University
Columbus, OH 43210

T. Lienert
Sandia National Laboratories
Albuquerque, NM 87185

ABSTRACT

The microstructure, mechanical properties and fracture characteristics of a pulsed Nd: YAG laser weld in a rapid solidification/powder metallurgy (RS/PM) Al-8wt.% Fe-2.3wt.% Mo alloy have been investigated. Results showed the high power density but low total energy input associated with pulsed Nd: YAG laser welding to promote extremely rapid fusion zone (FZ) cooling rates in the vicinity of 10^5 °C/s. The weld FZ microstructure consisted primarily of submicron-sized spherical dispersoids in a matrix of fine dendritic-alpha aluminum. A dispersoid-coarsened heat-affected zone (HAZ) was also observed in the boundary between successive, overlapping melt zones. Transverse-weld tensile testing found fracture to occur in the unaffected base metal indicating 100% weld joint efficiency. Longitudinal-weld bend ductility testing revealed fracture initiation and propagation to be associated with the HAZ between successive melt zones at a bend ductility level only marginally below that of the base metal.

AL-8FE-2MO REPRESENTS A NEW FAMILY OF dispersion-strengthened aluminum alloys with an "engineered" microstructure produced via rapid solidification/powder metallurgy (RS/PM) processing [1-5]. These alloys are characterized by novel hyper-eutectic Al-Fe base compositions with ternary and/or quarternary additions of Mo, Ce, Ni and Si to improve dispersoid stability at elevated-temperature. In these alloys, utilization of rapid cooling rates (in the range of 10^4 to 10^6 °C/s) suppresses the formation of primary intermetallic particles and instead promotes a solute supersaturated dendritic-alpha aluminum and/or micro-eutectic [2]. Subsequent consolidation and thermo-mechanical processing (TMP) treatments decompose the metastable as-solidified microstructural constituents and produce a high volume fraction of submicron-sized thermally stable dispersoids. The above microstructural features exhibit dispersion strengthening effects and consequently provide superior room-temperature and elevated-temperature mechanical properties [2, 4]. These high performance RS/PM Al-Fe-X alloys compete with Ti-6Al-4V alloy on a specific strength basis for use in several aerospace components operating at temperatures up to 315 °C [3-5].

If RS/PM Al-Fe-Mo type dispersion-strengthened alloys are to be utilized in structural applications, their efficient joining will be necessary. Considering the dependency of their superior mechanical properties on an "engineered" microstructure, it is apparent that joining techniques which can "recreate" and/or "retain" the unique microstructural characteristics of the base metal need to be utilized in order to achieve high joint efficiency. Among the fusion welding processes currently available to join aluminum alloys, high energy density processes such as electron beam (EB) and laser welding (LW) offer the greatest potential for achieving the above two microstructural goals. Recent weldability studies on Al-8wt.% Fe-2.3wt.% Mo (Al-8Fe-2Mo) determined that the high energy density and rapid cooling rates provided by EB welding generated an extremely fine FZ structure which exhibited a hardness and strength superior to that of the base metal [6]. However, the presence of a structurally coarse fusion boundary region (FBR) in these weldments served as a "weak-link" and promoted preferential failure with low ductility and a weld joint efficiency of 73%. Further EB welding investigations determined that the structurally coarsened FBR can be eliminated by using a lower weld energy input which promoted a steeper temperature gradient and a higher FZ cooling rate in excess of 10^4 °C/s [7]. These latter welds failed in the HAZ with acceptable ductility and an improved joint efficiency of 88%. Considering that an increased energy density could further increase the temperature gradient and cooling rate within the weld, and thereby enhance the FZ and HAZ microstructures, the present investigation was initiated in order to examine the microstructure, mechanical properties and fracture characteristics of a high energy density Nd: YAG pulsed laser weld in a RS/PM Al-8Fe-2Mo sheet.

EXPERIMENTAL PROCEDURE

The Al-8Fe-2Mo sheet utilized in this investigation originated from helium-atomized powder produced by Pratt and Whitney's rapid-solidification-rate (RSR) process [2, 4]. The inert atomization conditions produced spherically symmetric powder particles and also resulted in minimal oxidation and hydration of the powder particle surfaces. Subsequent to RSR processing, powder particles were

S. Krishnaswamy

---

compacted by direct consolidation, hot extruded into a billet and warm rolled into sheet 1.27 mm in thickness. The chemical composition of the as-received Al-8Fe-2Mo sheet was 8.0 wt.% Fe and 2.3 wt.% Mo with the residual hydrogen content below 1 ml/100 gm Al.

Autogenous Nd: YAG laser welds were produced with the weld longitudinal axis oriented parallel to the sheet rolling direction. The pulsed Nd:YAG laser welding conditions were optimized in order to produce a full-penetration, high depth-to-width ratio FZ. The optimized welding parameters were: 10 Hz pulsing rate, 5 ms pulse duration, 105 W (10.5 J/pulse) pulse power, 2.1 KW peak power, 2.54 mm/s (6 ipm) weld travel rate, 41.34 J/mm average energy input, 102 mm (4") focal length and argon shielding gas at a flow rate of 16.5 l/min. (35 cu. ft/hr). Subsequent to welding, the test coupons were evaluated using radiography to reveal possible weld defects such as cracks and porosity. Following radiographic examination, transverse and top sections of the weld coupons were mounted, polished and etched (Keller's reagent) for metallographic characterization using light microscopy.

Base metal and weldment microstructures were also characterized using thin foil transmission-electron microscopy (TEM). Thin foils for TEM characterization were prepared by jet-electropolishing technique using a solution of 1 part nitric acid in 3 parts methanol, at 20 V and at a temperature of -25 °C. Microstructure characterization was performed using a JEOL 200CX microscope operated at 200 KV. Additionally, energy dispersive spectrometer (EDS) analysis was performed using a Tracor-Northern TN 2000 system. A Cliff-Lorimer data analysis technique was utilized to obtain semi-quantitative compositions based on empirically determined K factors [8].

Base metal and weldment mechanical property evaluation included Vicker's diamond pyramid hardness (DPH) testing using a 500 gm load, transverse tensile testing (12.7 mm x 3.2 mm gage section) and longitudinal bend ductility testing. The longitudinal-weld bend ductility test was performed with the weld face in tension.

Fractography was performed on a Hitachi S-510 scanning-electron microscope (SEM) operated at 25 KV. Examination of the longitudinal weld bend coupon provided an "in-situ" comparative evaluation of the fracture in the FZ, HAZ and the unaffected base metal.

RESULTS & DISCUSSION

BASE MATERIAL CHARACTERIZATION - Light microscopy showed the as-received sheet to exhibit a uniform distribution of extremely fine, dark-etching dispersoid particles in a light-etching alpha aluminum matrix (Figure 1A). Dark-etching stringers were occasionally observed oriented parallel to the sheet rolling direction. These stringers appeared to originate from coarse powder particles which contained primary intermetallic particles [2], rather than from oxides present on powder particle surfaces.

TEM analysis of the base material microstructure revealed sub-micron dispersoids which varied significantly in size and morphology (Figure 1B). Although specific dispersoid types were not identified using electron diffraction techniques, EDS composition analysis indicated the coarser dispersoids to be Al_6Fe type, which is a metastable intermetallic previously reported in rapidly solidified Al-Fe-Mo and Al-Fe alloys [2, 9]. An alpha grain size of 1 to 2 μm was also indicated by bright and dark field imaging.

Mechanical property testing performed on the base metal found a hardness of 120 DPH, an ultimate tensile strength of 376 MPa (54.5 Ksi), a tensile elongation of 11% and a longitudinal bend ductility of 14 %.

WELD INTEGRITY - Radiographic examination of the welded coupons did not reveal indications of cracking. Although occasional spherical pores were observed within the FZ, the porosity levels were well within allowable limits for aerospace applications.

WELD STRUCTURE CHARACTERIZATION - Figures 2A & 2B show the macrostructure of the transverse and top sections of the pulsed Nd: YAG laser weld. As indicated, the FZ consisted of a light-etching microstructure with curvilinear bands of a dark-etching microstructure bounding successive melt zones. Light microscopy analysis of the light-etching region at increased magnification (Figures 3A and 3B) revealed extremely fine particles in an alpha aluminum matrix. Variations in the distribution of these dispersoid particles in the form of "swirls" appeared to be associated with convective fluid flow patterns experienced in the melt prior to solidification. The dark-etching regions observed at the boundaries between successive melt zones exhibited a smooth interface with the original melt zone and an irregular interface

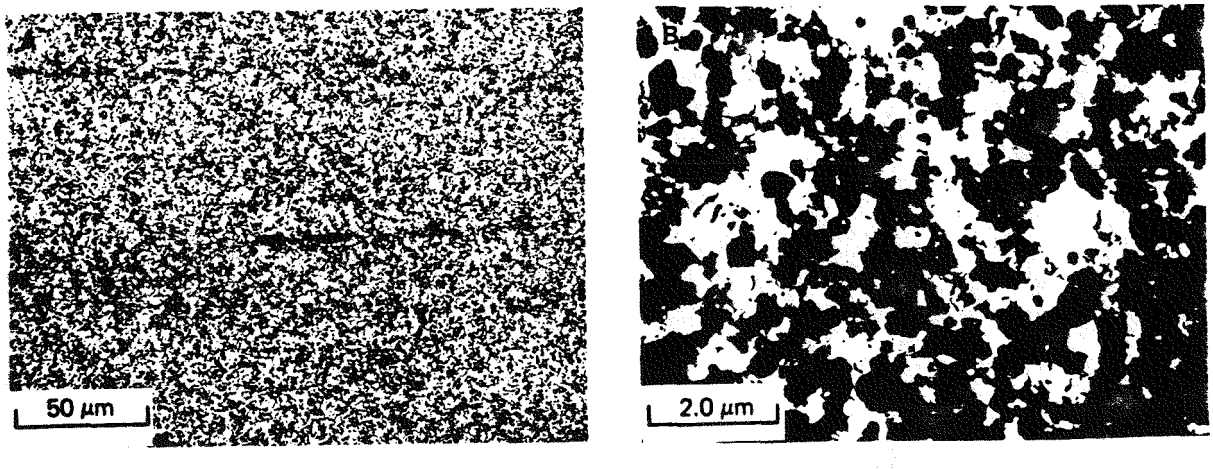

Figure 1: (A) Light micrograph and (B) TEM micrograph of RS/PM Al-8Fe-2Mo base metal.

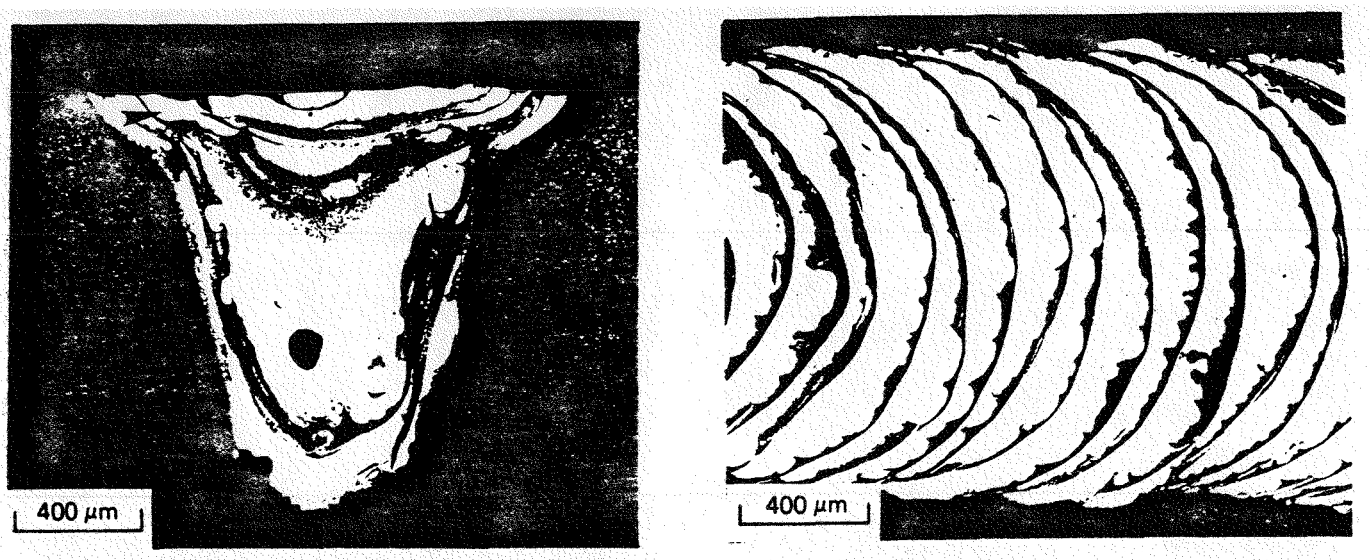

Figure 2: Light micrographs of pulsed Nd:YAG laser weld in Al-8Fe-2Mo showing (A) transverse section, (B) top surface. Arrows in (A) indicate locations of hardness traverses shown in Figure 5.

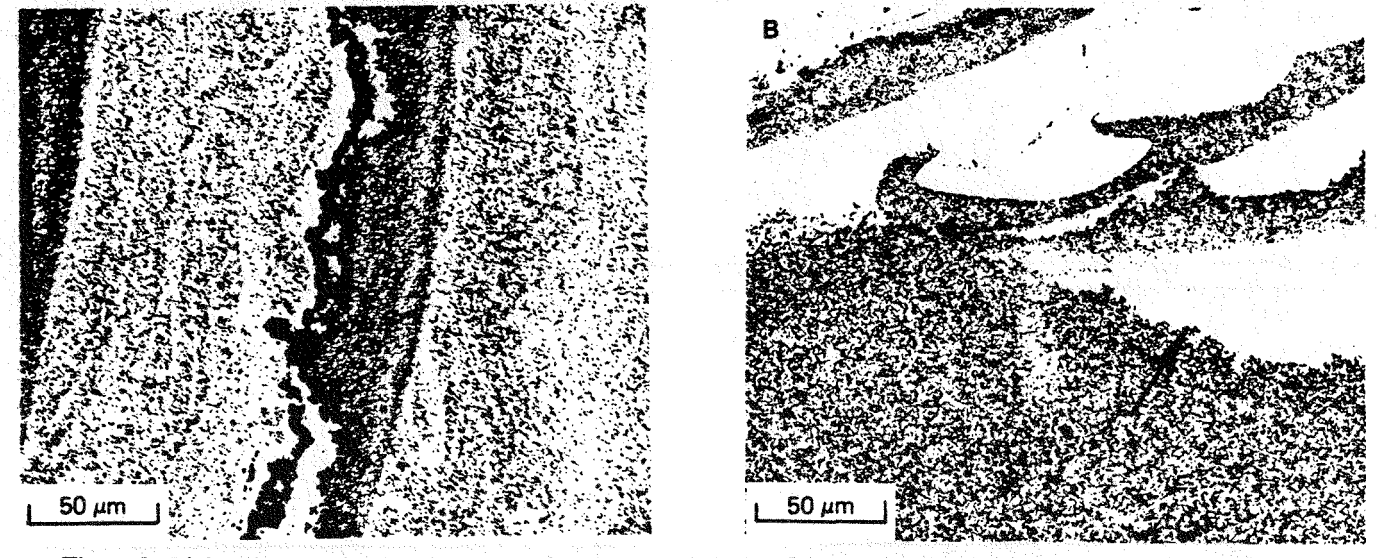

Figure 3: Light micrographs showing top surface of pulsed Nd:YAG laser weld in Al-8Fe-2Mo: (A) center of FZ, (B) fusion boundary (arrow).

bounding the subsequent melt zone. As shown in Figures 2B and 3B, the irregular boundary frequently exhibited a macroscopically "cusped" appearance, which was attributed to the nature of fluid flow within the molten weld pool. Analysis of this dark-etching structure at increased magnification suggested that it comprised of a HAZ on the side of the original melt zone and a FBR on the side of the subsequent melt zone. Solid-state dispersoid coarsening was evident within the HAZ, while in the FBR dispersoids coarsened in a stagnant region of molten alpha aluminum [6]. Evidence of a narrow, dark-etching band in the base metal directly adjacent to the FZ indicated a dispersoid-coarsened HAZ (Figure 3B).

TEM analysis of the weldment more clearly characterized the weld FZ and HAZ microstructures. As shown in Figures 4A and 4B, the FZ consisted of spherical intermetallics in a matrix of fine dendritic alpha aluminum. EDS analysis indicated that these intermetallics were the Al_6Fe type. The size and morphology of these intermetallics and their Al_6Fe type composition suggested that these particles originated from the base metal dispersoid particles. Based on this observation, it is apparent the weld "fusion zone" was essentially a partially-melted region comprised of dissolving dispersoid particles in molten aluminum. Observed differences in the size and distribution of the intermetallics were attributed to the variations in the thermal conditions experienced within the molten weld pool, with dispersoids experiencing high temperatures dissolving more extensively than those in lower temperature regions. As shown earlier in the light micrographs (Figures 3A & 3B), convective currents within the FZ controlled the movement of dispersoids through these "high" and "low" temperature regions in the weld pool and thereby influenced their final size and distribution. Solidification of the weld pool initiated epitaxially from the fusion boundary, with columnar alpha-aluminum grains effectively "entrapping" the unmelted/undissolved dispersoids as solidification proceeded along a relatively steep temperature gradient. As shown in Figures 4A and 4B, solidification of the alpha aluminum matrix occurred to a cellular-dendritic substructure with fine intermetallics located in the last-to-solidify dendrite intersticies. EDS

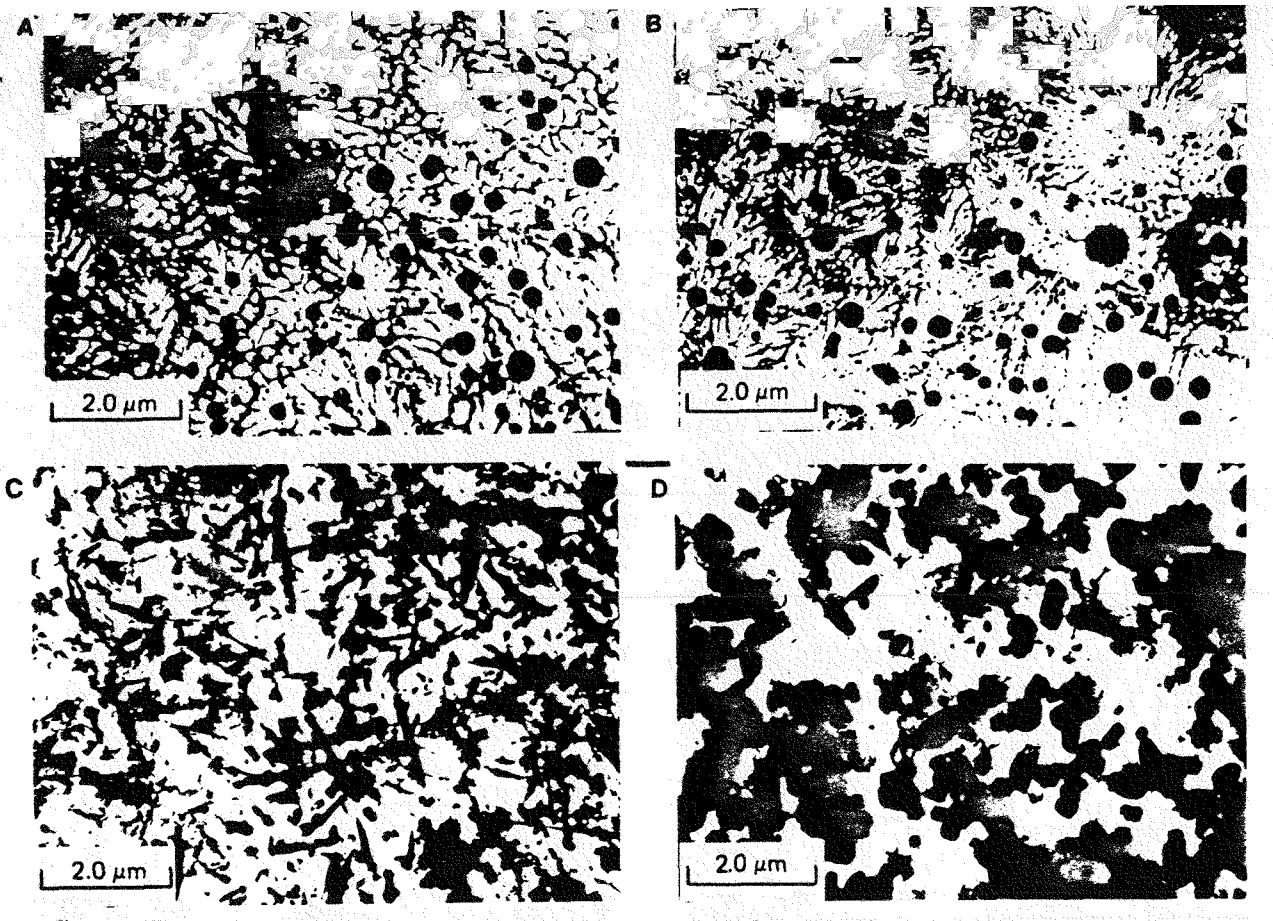

Figure 4: TEM micrographs of pulsed Nd:YAG laser weld in Al-8Fe-2Mo: (A) fusion zone adjacent to fusion boundary, (B) center of FZ, (C) HAZ within FZ, (D) HAZ in base metal.

semi-quantitative compositional analysis of the overall dendritic structure showed an Fe content of about 6wt.%, which was well beyond the eutectic composition of 1.8wt.% Fe [10] in binary Al-Fe systems (albeit Mo additions influence this composition to a limited extent). The solidification of this hyper-eutectic composition to primary alpha with an Fe content of about 0.85wt.% (versus a maximum equilibrium solid-solubility limit of 0.04 wt.% Fe [10] at the eutectic temperature) was attributed to the rapid cooling and solidification rates experienced within the pulsed laser weld. A comparison of the dendrite spacings with previous relationships between dendrite spacing and cooling rate in aluminum alloys [11, 12] indicated a Nd: YAG laser weld cooling rate of about 10^5 °C/s through the solidification temperature range. Nearer to the center of the FZ, where the temperature gradient became shallower, evidence of equiaxed growth was apparent. In this region, relatively coarse dendritic alpha-aluminum nucleated directly upon the spherical intermetallics.

Analysis of the HAZ in the FZ between successive laser pulses revealed the formation of acicular intermetallics believed to be Al_3Fe type [2, 9] in an alpha aluminum matrix (Figure 4C). Although occasional spherical intermetallics were also observed in this region, the cellular-dendritic solidification structure was completely absent. During the laser weld thermal cycle, the extremely fine intermetallics at dendrite intersticies apparently underwent preferential dissolution in solid-state and thereby provided solute flux for the formation of acicular intermetallics. The supersaturated alpha aluminum matrix might have also provided additional solute flux for the formation of these acicular particles.

Figure 4D shows the TEM microstructure of the HAZ in the base metal directly adjacent to the FZ, and indicates only slight coarsening of the dispersoids versus the unaffected base metal (Figure 1B).

WELD PROPERTIES - Figure 5 shows hardness traverses at two locations across the transverse weld cross-section shown in Figure 2A. Consistent with the microstructural analysis, the hardness of the light-etching regions near the weld center was appreciably greater than that of the base material (220 versus 120 DPH). Hardness levels decreased to 170 DPH in the dark-etching boundary between successive pulse melt zones within the FZ due to appreciable coarsening of the dispersoids in this region. The hardness decreased to 118 DPH in the narrow HAZ in the base metal which was only marginally below that of the base metal.

Fracture of the transverse-weld oriented tensile specimens occurred in the unaffected base metal, indicating a 100% joint efficiency. Tensile properties of four tensile specimens averaged an ultimate tensile strength of 374 MPa (54.2 Ksi) and an elongation of 11%. The occurrence of fracture remote from the weld FZ, despite the presence of a HAZ exhibiting a lower hardness than the base metal, was attributed to the minimal width of the HAZ and the constraint effects of the surrounding higher

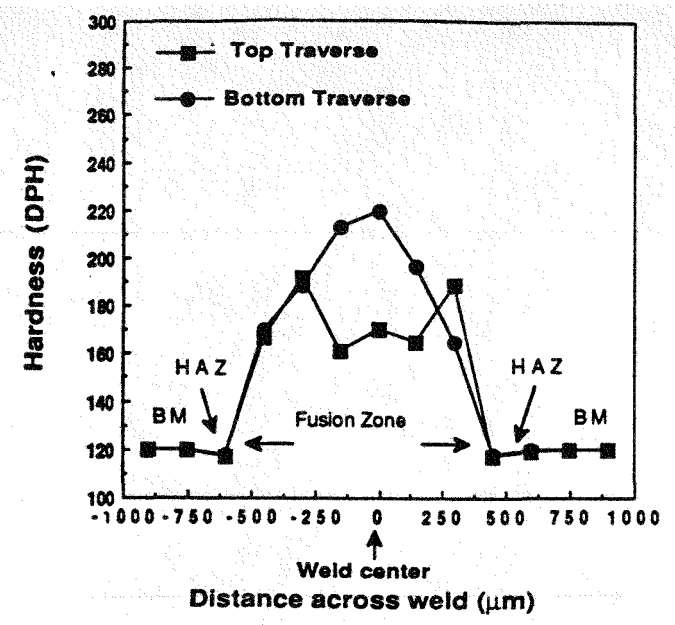

Figure 5: Hardness traverses across pulsed Nd:YAG laser weld in Al-8Fe-2Mo (location of top and bottom traverses are shown in Figure 2A).

strength microstructure. Longitudinal-weld bend ductility testing indicated a 11% bending strain at fracture initiation, which was only marginally below that of the base metal.

FRACTURE CHARACTERISTICS - Examination of the top surface of the fractured longitudinal-weld bend specimen (Figure 6) found the marginal reduction in bend ductility to be associated with the presence of the dispersoid-coarsened HAZ within the weld FZ. Although a specific crack initiation site could not be identified, crack propagation occurred principally along the smooth interface between the HAZ and the preceding pulse, rather than entirely through the coarsened HAZ or along the more irregular fusion boundary interface with the succeeding pulse. As shown in Figure 6, near the edges of the FZ the crack path deviated from the curvilinear boundary to a direction oriented perpendicular to the direction of maximum tensile stress.

SEM fractographic analysis of the longitudinal-weld oriented bend specimen showed ductile-appearing fracture in the base metal regions which was consistent with the nucleation, growth and coalesence of microvoids in the interface between the dispersoid particles and the relatively soft alpha aluminum matrix (Figures 7A & 7B). Although the macroscopic fracture path in the base metal indicated a texture parallel to the sheet rolling direction (Figure 7A), the size of the microvoids generally appeared to be uniform. Fracture in the weld FZ also occurred in a ductile manner by void formation (Figures 7C & 7D). However, the size of the voids varied appreciably across the fracture surface. In some locations, voids were larger than those in the base metal, which was consistent with the generally lower distribution of intermetallics in the FZ (i. e., compare Figures 1B and 3A). However, in other locations a void size finer than that observed in the base metal was found, suggesting a possible influence from interdendritic intermetallic particles in promoting void nucleation. Clearly, the observed variations in void size across the FZ were consistent with variations in intermetallic distribution within this region. Analysis of the fracture initiation region at the top surface of the bend specimen (along the HAZ boundary within the FZ) revealed no unique characteristics.

Figure 6: Light micrograph showing fracture path on top surface of longitudinal-weld oriented bend specimen in Al-8Fe-2Mo. Arrow indicates direction of maximum tensile stress during bend testing.

SUMMARY

The results of this investigation determined that the rapid cooling rates provided by pulsed Nd: YAG laser welding promoted a FZ microstructure comprised of submicron intermetallics in a matrix of fine dendritic alpha aluminum and minimal dispersoid coarsening in the base metal HAZ. The high strength of this FZ microstructure and the narrow width of the HAZ provided 100% joint efficiency. A dispersoid-coarsened microstructure in the HAZ at the boundary between successive melt zones served as a preferential fracture path during bend testing but promoted only a minimal loss in ductility.

ACKNOWLEDGEMENT

Research performed at The Ohio State University was supported by the Army Research Office under contract # DAAL03-88-K-0049. Work conducted at Sandia National Laboratories was supported by the Department of Energy under contract # DE-AC04-76DP00789. The authors also express appreciation to Mr. H. O. Colijn at the Central Electron Optics Facility, OSU for his assistance in EDS analysis.

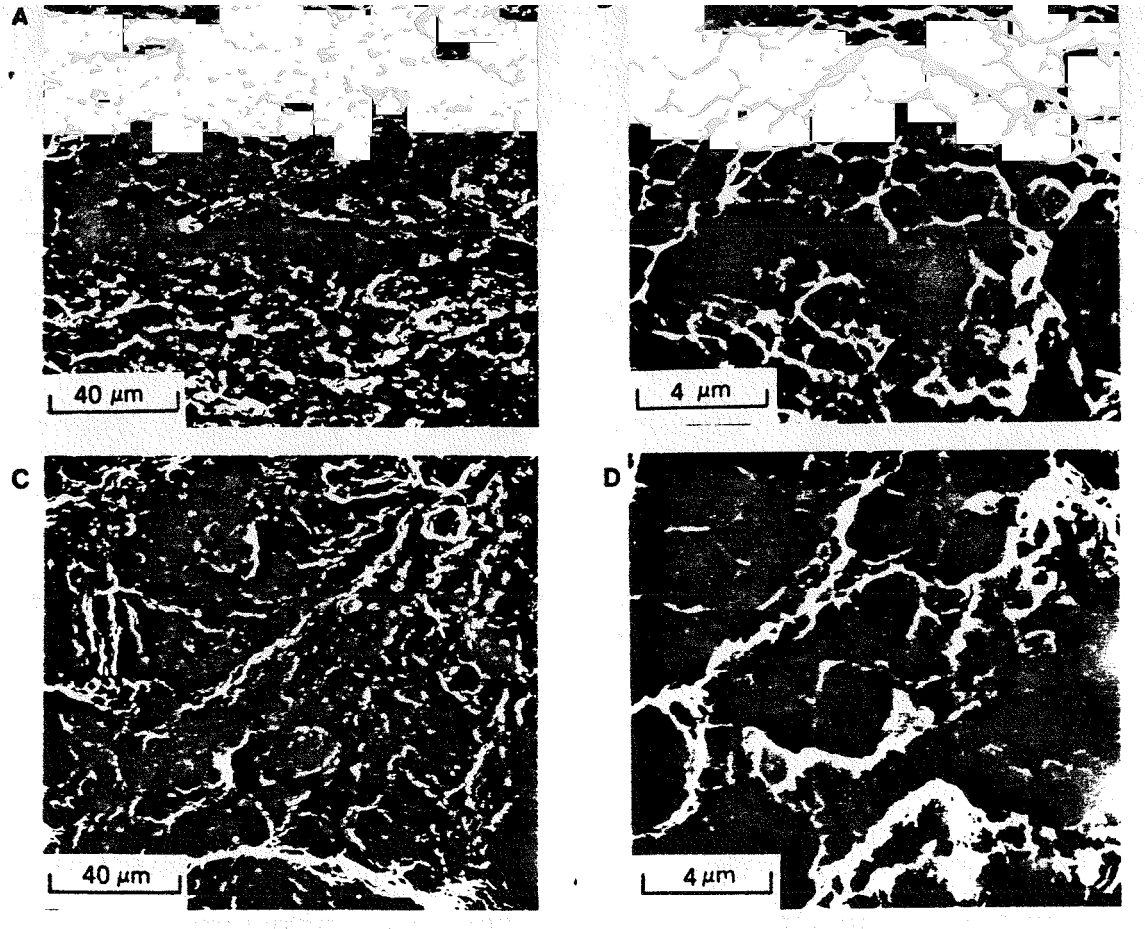

Figure 7: SEM fractographs of longitudinal-weld oriented bend specimen in Al-8Fe-2Mo: (A, B) unaffected base metal, (C, D) center of FZ.

REFERENCES

1) S. L. Langenbeck, W. M. Griffith, G. J. Hildeman and J. W. Simon, in "Rapidly Solidified Aluminum Alloys, STP 890," M. E. Fine and E. A. Starke, Jr. Eds. ASTM, PA, 410-22, (1986).

2) C. M. Adam and R. G. Bourdeau, in "Rapid Solidification Processing: Principles and Technologies II," R. Mehrabian, B. H. Kear and M. Cohen, Eds. Claitors Publishing, Baton Rouge, LA, 246-59, (1980).

3) C. M. Adam, in "Science and Technology of Undercooled Melts," P. R. Sahm, H. Jones and C. M. Adams, Eds. NATO-ASI Series, Martinus-Nijhoff Publishers, Dodrecht, 186-209, (1986).

4) C. M. Adam, in "Rapidly Solidified Amorphous and Crystalline Alloys, Vol. 8," B. H. Kear, B. C. Giessen and M. Cohen, Eds. Elsevier Science Publishing Co. 411-22, (1982).

5) C. M. Adam, in "Mechanical Behavior of Rapidly Solidified Materials," S. M. L. Sastry and B. A. MacDonald, Eds. TMS, Warrendale, PA, 21-39, (1985).

6) W. A. Baeslack III and S. Krishnaswamy in "International Trends in Welding Research," S. A. David, Ed. ASM International, Metals Park, OH, 357-62, (1986).

7) S. Krishnaswamy and W. A. Baeslack III, Matls. Sci. & Engg. 98, 137-41, (1988).

8) M. H. Jacobs, A. G. Doggett and M. J. Stowell, J. Matls. Sci. 9, 1631-43, (1974).

9) P. Trebbia, "CLEDX: a stand alone program for quantitative X-ray analysis of thin films using the C-L procedure," to be published in a forthcoming issue of Ultramicroscopy.

10) L. F. Mondolfo, Aluminum Alloys: Structure and Properties, Butterworths, London, 24, (1976).

11) H. Jones, "Rapid Solidification of Metals and Alloys," Monogr. 8, Institution of Metallurgists, London, 40-43, (1982).

12) G. R. Armstrong and H. Jones in "Proc. conf. Solidification and Casting of Metals," Sheffield, The Metals Society, London, 454-59, (1979).

DISCLAIMER